

*Summing up*, the skeleton response to many quasi-static reversals can be captured with rate-independent asymptotic state cycles including the hidden force-roughness, transitions to them may be interpreted as intermittent creep or relaxation. An unknown initial force-roughness is swept out by suitable deformations up to attractors, thus the force-roughness gets determined although it cannot be observed. Cyclic deformations cause a gradual loss of the mean stress deviator, whereas the mean skeleton pressure can tend to a decay or to a lower stationary value. Ratcheting leads to a lower than critical mean stress obliquity, whereas the mean pressure can increase or decrease according to the void ratio. Asymptotic state cycles exhibit pulsations of pressure or void ratio with twice the frequency of reversals, this could also hold true for the hidden force-roughness.

#### 4.4 Elastoplasticity with back stress

We consider first psammoid RSEs with cylindrical symmetry. According to Manzari and Dafalias (1997) they may have the following elastoplastic properties, Fig. 4.4.1. A narrow conical elastic range is assumed with its apex at the origin in the plot of  $\sigma'_1$  vs.  $\sqrt{2}\sigma'_{s2}$  (a). Its mean direction  $\psi_\alpha$  is the only internal state variable, it may be called *back stress direction*. The cone width is assumed to be a material constant, which is rather arbitrary as sand has at best an infinitesimal elastic range.

Within the elastic range the hypoelastic relations

$$\begin{aligned} \text{(a)} \quad \dot{\varepsilon}_1 - \dot{\varepsilon}_2 &= \dot{\varepsilon}_1^e - \dot{\varepsilon}_2^e = G_r(p'/p_r)^m (\dot{\sigma}_{s1} - \dot{\sigma}_{s2}) \\ \text{(b)} \quad \dot{\varepsilon}_1 + 2\dot{\varepsilon}_2 &= \dot{\varepsilon}_v = \dot{\varepsilon}_v^e = K_r(p'/p_r)^m (\dot{\sigma}_{s1} + 2\dot{\sigma}_{s2}) \end{aligned} \quad (4.4.1)$$

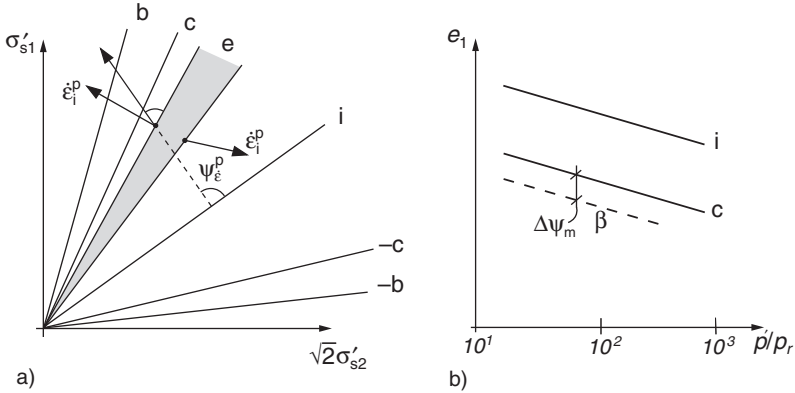


**Fig. 4.4.1.** Stress ranges (a) and related void ratios (b) of a cylindrical psammoid RSE in the model by Manzari and Dafalias (1997)

are assumed, then strain rates are elastic ( $\dot{\varepsilon}_i = \dot{\varepsilon}_i^e$ ). The exponent is taken as  $m = 1/2$ , the reference moduli are related with a Poisson ratio  $\nu < 1/2$  via

$$K_r/G_r = (1 + \nu)/(1 + 2\nu) \quad (4.4.2)$$

The reference pressure in (4.4.1) is chosen at will, e.g.  $p_r = 100\text{kPa}$ . Equation (4.4.1a) suits to (4.2.1), thus the dependence of  $G_r$  on  $e$  could be allowed for, but the anisotropy explained with Fig. 4.2.2 is neglected. Equation (4.4.2) was also used by Pradhan et al. (1989) for the evaluation of triaxial test results which are shown in Sect. 4.2. As outlined with Fig. 4.2.3 the parameters in (4.4.1) cannot be determined precisely: an elastic range does not really exist, its choice is inevitably arbitrary.

Plastic strain rates  $\dot{\varepsilon}_i^p = \dot{\varepsilon}_i - \dot{\varepsilon}_i^e$  occur when the stress point leaves the elastic range. Two flow rules are assumed for the ratio  $\dot{\varepsilon}_2^p/\dot{\varepsilon}_1^p$ , or the direction  $\psi_\varepsilon^p$  instead (Fig. 4.4.1a). Rowe's (1962) stress-dilatancy rule (2.2.20) is taken for deviatoric loading, i.e. for increasing  $|\psi_s|$ . A contractancy of bigger amount than the dilatancy for loading is assumed for deviatoric unloading, i.e. a bigger  $|\psi_\varepsilon^p|$  for decreasing  $|\psi_s|$ . In both cases  $\psi_\varepsilon^p$  depends on  $\psi_s$ , but not on  $e$ . This double flow rule corresponds to what Pradhan et al. (1998) found by triaxial tests with reversals, cf. Fig. 4.2.3.

Two hardening rules are needed for volumetric and deviatoric parts. Assuming isochoric grains the void ratio changes with the skeleton volume by (2.2.10) as for simple psammoids. The back stress angle  $\psi_\alpha$  changes alongside with the one of stress in case of plastic deformations by a relation of  $\psi_\alpha$  with  $\psi_\alpha$ ,  $\psi_s$  and the state parameter  $\psi_e$  shown in Fig. 4.4.1b which replaces  $e$ . An increase of  $|\psi_\alpha|$  is limited by the CSSM bounding cone for the actual  $e$ , it gets wider by contraction. Plastic strain rates for stress paths with constant direction  $\psi_s$  inside the CSSM bounding cone are neglected in Manzari and Dafalias' (1997) model. This is completed by an interpolation with the requirement of continuous elastoplastic transitions (consistency condition).

Gajo and Muir Wood (1999) proposed an extension of this model. Using the CSSM-frame for state boundaries, they work also with Been and Jefferies' (1985) state parameter and the hypoelastic relations (4.4.1). The elastic range consists of a cone as in Fig. 4.4.1a and a cap like the one by CSSM. Two different flow rules are again employed for the cone flanks, the related hardening rules are kinematic and volumetric. Additional flow and hardening rules are proposed for the assumed cap, they depend on  $e$  and  $p'$ . The back stress has thus one more component than the model introduced with Fig. 4.4.1. In both models the back stress characterizes an elastic range inside the one by CSSM, thus they resemble Mróz' (1967) model for solids (Fig. 4.1.8). Interpreting the back stress as a representation of force-roughness, the one shown with Fig. 4.4.1 neglects the barotropy for the hidden state as for a solid (Sect. 4.1), whereas this barotropy is captured by Gajo and Muir Wood (1999).

Pestana and Whittle (1999) propose similar relations. In a stress plane the elastic ranges are bounded by a bullet-like curve as in Fig. 2.3.2b. Skew lemniscates are employed so that tensile stresses are excluded, and so that critical

stress obliquities correspond to the same friction angle for axial shortening and lengthening. The direction of plastic strain rates (flow rule) is associated (normality rule) for increasing pressures, and non-associated by different stress-dilatancy relations for increasing and decreasing stress obliquities. Changes of the back stress values, which characterize the variable elastic range, are related with plastic strain rates by kinematic and volumetric hardening rules. Hypoelastic relations like (4.4.1) are assumed for the elastic range. As always with elastoplastic relations the amount of plastic strain rate is determined by the continuity of response for elastoplastic transitions (consistency).

Algebraic representations of such elastoplastic relations with back stress ( $\text{elp-}\alpha$ ) are intricate already in case of cylindrical symmetry. Publications are rarely so tractable that one could write a computer code, and it is difficult to discover subtle defects. Variants were proposed with improvements, but it is hard to understand them in all detail. Given a complete and consistent set of equations or even a computer code, one is still left alone with the calibration of material parameters. Given a computer code and a realistic range of parameters, however, one could judge such constitutive relations *more geometrico* by means of attractors. The following plots were produced by Niemunis and Prada (2010) with a more recent  $\text{elp-}\alpha$  by Taiebat and Dafalias (2007), called *Sanisand*, which works with a second tensorial hidden variable and had to be corrected in some details for getting feasible. Authors of similar theories should provide software with instructions in their homepage so that potential users can judge the range of validity without getting confused by intricate algebra and numerics. If simulated attractors are realistic they may be used for the calibration of parameters.

Evolutions by  $\text{elp-}\alpha$  with *proportional deformations* look like Fig. 4.3.6. The asymptotic state limits are the same as without back stress (Sect. 2.3). A plot of void ratio vs. log pressure shows the evolution of two key state parameters, but not the one of back stress. A plot of back stress obliquity vs. stress obliquity would reveal a gradual adaption well before state limits are attained. This means that the rather arbitrary initial back stress is swept out by a sufficient deformation, thereafter the response gets determinate as is the hidden state.

Turning to *reversals*, we consider first evolutions of saturated cylindrical RSEs with *free drainage*. Figure 4.4.2 shows a simulation of Jefferies' (1997) experiment which was plotted in Fig. 2.6.4. The stress-strain curve (a) and the plot of volumetric vs. axial strain (b) are partly realistic. The deviatoric deformation by un- and reloading is fairly well captured except for the approach to the previous deviator. A peak state with maximal dilation is not obtained as in the experiment. The calculated elastic dilation just after the onset of deviatoric unloading is less realistic than the subsequent contraction with further unloading. The further contraction and the following dilation by reloading is well captured. The elastic dilation just after unloading could be avoided with another hypoelastic relation.

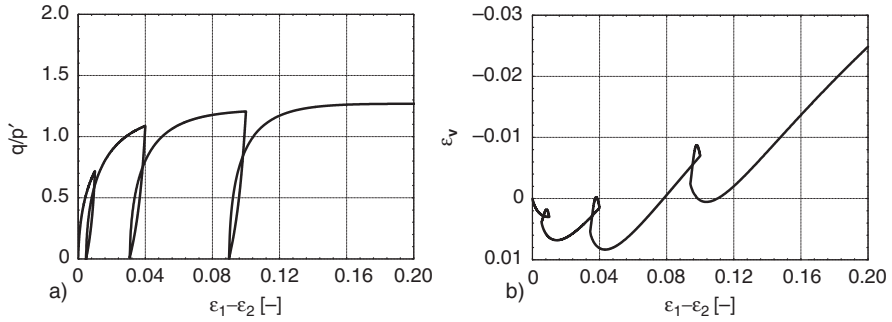


**Fig. 4.4.2.** Simulation of Jefferies' (1997) drained triaxial tests with reversals (Fig. 2.6.4) with Sanisand (Niemunis and Prada 2010); stress ratio (a) and volumetric strain (b) vs. deviatoric strain

The observed evolutions near the end of reloading are not apt for such evaluations as Jefferies' (1997) triaxial tests imply a loss of uniformity at least near state limits. Slender samples with rough endplates get less deformed near the plates (conical dead zones) and more than the average in the middle (bulges and shear bands, Sect. 14.1). The reported sharp bends at the end of reloading suggest the verge of an elastic range, but the observed simultaneous volume changes are markedly anelastic. It appears that the reloaded sample is stiffer by a kind of eigenstress from the rough plates, and that the sharp bend is due to a spontaneous shear localization. The peak is exaggerated therefore in standard tests. Sanisand cannot reproduce these effects if uniformity is assumed, but simulations without it will be cumbersome or hardly feasible with localization.

Even with short samples and lubricated endplates a loss of uniformity cannot be avoided near state limits (Sect. 14.1). Wu (1992) obtained similar results as Jefferies (1997) with short samples and lubrication. He did not observe shear bands, but a diffuse bifurcation near the plates (Sect. 14.1). Patterns of shear bands need not appear at the confining membrane, but they arise inevitably with overcritical stress obliquities (Sect. 8.2). Unloading from a state with shear bands means that these are contracted by reverse shearing, this could explain the overall contraction with high stiffness in Wu's and Jefferies' tests. Reloading can lead to a sudden reactivation of dilating shear bands, this could explain the high stiffness before and its sudden drop after the end of reloading observed by both authors. Evaluations without localizations are evidently misleading if they really happen. The polarization needed to determine the thickness of shear bands means a higher force-roughness (Sect. 8.2), this cannot be covered by a hidden variable like back stress in  $\text{elp-}\alpha$ .

We consider now simulated evolutions of *undrained* saturated cylindrical RSEs. Figure 4.4.3 shows that the findings with *one reversal* by Verdugo and Ishihara (1996), which were plotted in Fig. 2.6.2, can be well reproduced. The

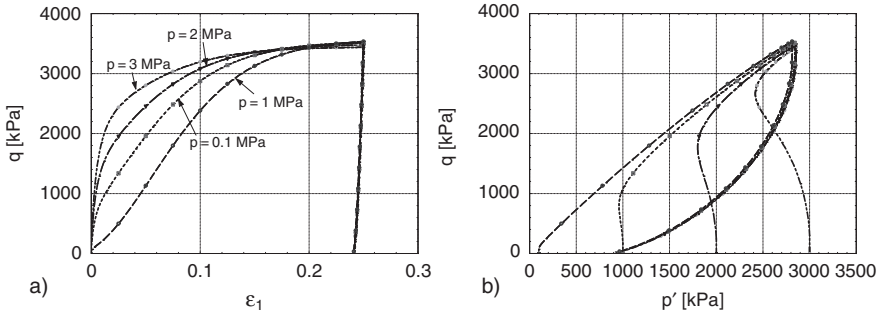


**Fig. 4.4.3.** Simulation of undrained triaxial tests (Verdugo and Ishihara 1996) with one reversal (Fig. 2.6.2) by means of Sanisand (Niemunis and Prada (2010); deviatoric stress vs. axial shortening (a) and vs. effective mean pressure (b)

onset was isotropic with different pressures for the same void ratio  $e$ , the initial back stress was estimated by simulating previous evolutions with drainage. With a suitable  $e$  the stress-strain curves (a) depend on the initial pressure as observed, lead to the same critical state and have a single unloading branch. The stress paths (b) start without change of mean pressure  $p'$ , exhibit then a reduction of  $p'$  and tend to a common point on the critical line as observed. The calculated paths for unloading do not reproduce the immediate pressure reduction, this lack could be removed with a better hypoelastic relation. As outlined with Fig. 2.6.2 the subsequent reduction of  $p'$  is reduced by the decreasing membrane penetration, its reproduction by Sanisand is even more realistic than suggested by the plots. Shear bands may be neglected as the evolution remained in the subcritical range.

A simulation of Wichtmann's (2005) undrained triaxial tests with an *alternating deviator* of stress is plotted in Fig. 4.4.4. The skeleton is rather dense and isotropic at the onset, the initial back stress is guessed. The stress path (a) tends to a stationary double cycle with temporary critical obliquities as in Fig. 2.6.6a. As outlined with the same figure this attractor is flatter than the observed one as the latter is distorted by the variable penetration of grains into the membrane. After a deviatoric preloading the transition to this attractor requires more reversals as observed. The deviatoric stress-strain curve exhibits an increasing hysteresis up to a loop with changing sign of curvature between reversals. This was similarly observed by Hyodo et al. (1989), the sample decayed likewise repeatedly in these experiments. The calculated cumulative deviatoric strain appears to be negligible, observed ones were not reported.

The above simulations suggest that 'Sanisand' as representant of  $\text{elp-}\alpha$  is well validated. It is unable, however, to reproduce the *intermittent relaxation* by small isochoric strain cycles shown in Fig. 4.2.6. Niemunis and Prada (2010) obtain thus first a gradual reduction of stress components, but the mean value  $p'$  does not converge to zero for any initial void ratio  $e$ . This shortcoming is

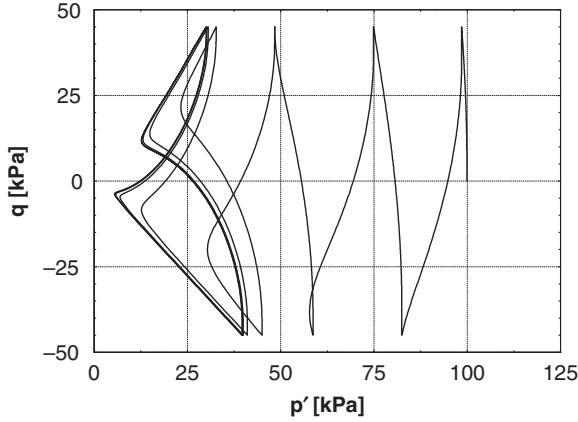


**Fig. 4.4.4.** Simulation of Wichtmann's (2005) undrained triaxial tests with symmetric deviatoric stress cycles (Fig. 2.6.6a) with Sanisand (Niemunis and Prada 2010)

due to the assumed  $p'$ -dependence of limit void ratios by CSSM (Sect. 2.3) without a lower bound. It could be avoided by using Bauer's (1996) formula (2.4.1) including the lower bound  $e_d$ .

An evolution up to a rather realistic *ratcheting* is obtained by Sanisand with an undrained RSE under a pulsating stress deviator, Fig. 4.4.5. The skeleton cannot decay temporarily with the employed limit void ratios by CSSM, the initial stress may be isotropic, an initial back stress is chosen at will in the allowed range. The stress path (b) tends to a lense which touches the line of critical obliquity, the deviatoric stress-strain curve tends to a stationary ratcheting (a). Both plots resemble Fig. 2.6.7a, b from triaxial tests by Hyodo et al. (1989), but the anelastic response is exaggerated by Sanisand. It appears that the deviations cannot be avoided with the same data set which produces

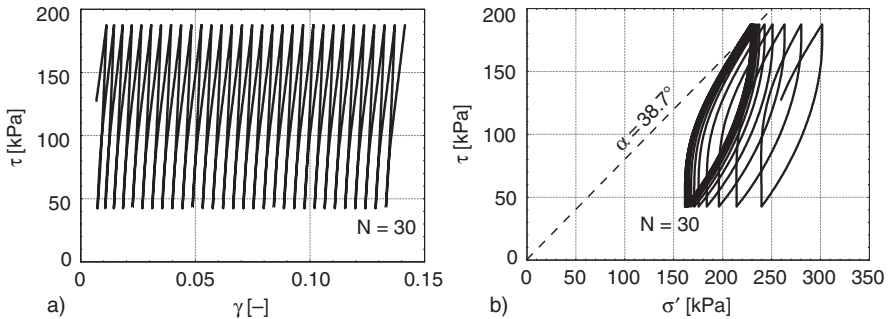


**Fig. 4.4.5.** Simulation of Hyodo's et al. (1989) undrained triaxial tests with one-sided deviatoric stress cycles (Fig. 2.6.7) with Sanisand (Niemunis and Prada 2010); (a) stress-strain curve, (b) stress path

a reasonable fit in the first two simulations shown above. The influence of the variable membrane penetration on the attainable agreement is not yet known.

The extension of elastoplastic relations with back stress to *cuboidal deformations* is straightforward in principle, but intricate in detail. Niemunis and Prada (2010) detected that Sanisand can produce a discontinuous response to changing directions in the deviator plane. This may be attributed to an artificial loss of stability with the intricate equations. Therefore it was not possible to reproduce cuboidal test results with reversals as the ones given in Sect. 2.8. The models by Gajo and Muir Wood (1999) and by Pestana et al. (2002b) cannot be judged in that respect as the papers are not fully tractable and as software for simulations is not freely available.

As *simple shearing* requires four stress components (Sect. 2.9) three back-stress components arise in Sanisand (and a fourth one with a cap). The assumed elastic range is a narrow hyper-cone with constant width and variable axial direction which is bounded by state boundary surfaces. The evolution of the hidden back stress with plastic deformations is modelled by a rather intricate combination of kinematic and volumetric hardening, this could hardly be represented graphically by projections. Two different flow rules are again assumed for increasing and decreasing stress obliquity, with the additional directional freedom this requires arbitrary specifications and caution for changing path directions. As with less degrees of freedom the assumed elastic response depends only on  $p_s$  and  $e$ , and the intensity of plastic deformations is determined by the requirement of continuity.

Simulations of the *alternating torsion* tests with saturated sand by Pradhan et al. (1989), which were given in Fig. 2.10.1, are shown in Fig. 4.4.6. With loose sand the nested hysteresis loops (a) are fairly well reproduced, but the strain path (b) exhibits an unrealistic sudden change of drift. With dense sand the nested loops are not as well captured (c) and the calculated strain path (d) shows an exaggerated dilation. The latter is due to shear localization for overcritical stress obliquities (Sect. 8.2). The observed interchange of dilation and contraction before and after reversals, respectively, is qualitatively reproduced. This unrealistic change of drift may be attributed to the unstable response mentioned above, it cannot be deduced from or easily removed in the Sanisand equations.

The response of sand to *isobaric shear cycles* as observed by Youd (1972) and shown in Fig. 2.10.3 cannot be reproduced with Sanisand (Niemunis and Prada 2010). This lack could be overcome with a lower bound void ratio  $e_d$ . Youd's tests with big amplitudes may be left aside as with them the stress obliquity got repeatedly overcritical so that shear bands arose. His tests with undercritical obliquities, however, may serve as a benchmark attractor as the inevitable non-uniformity is repeatedly reduced by reversals which break force chains.

Niemunis and Prada (2010) simulated also the *isochoric cyclic shear* test with a thick-walled cylinder by Ishihara and Towhata (1983) which was depicted in Fig. 2.10.6. The given alternating deviator without drainage leads

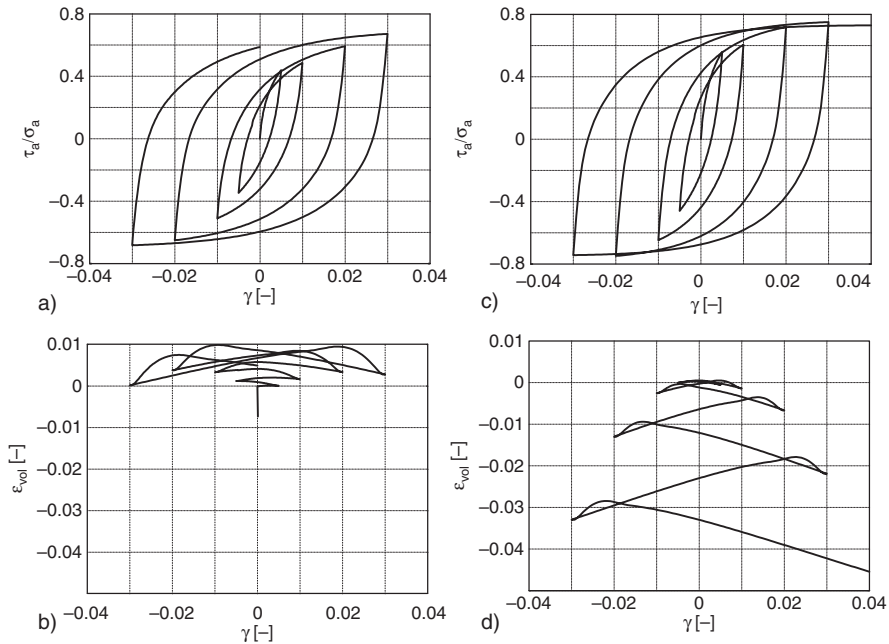


**Fig. 4.4.6.** Simulation of Pradhan's et al. (1989) drained hollow cylinder tests with increasing alternating torque (Fig. 2.10.1) with Sanisand (Niemunis and Prada 2010); stress ratio (a) and volume change (b) vs. shear strain for loose sand, same for dense sand (c, d)

to a butterfly with Sanisand, Fig. 4.4.7a, with an apparently realistic stress path. However, as outlined with Fig. 2.6.5 the observed attractor is widened and shifted by the penetration of grains into the membrane. The simulated hysteresis curves (b) are apparently close to the observed ones, but distorted by membrane penetration and temporary decay. Sanisand parameters were apparently adapted to such tests.

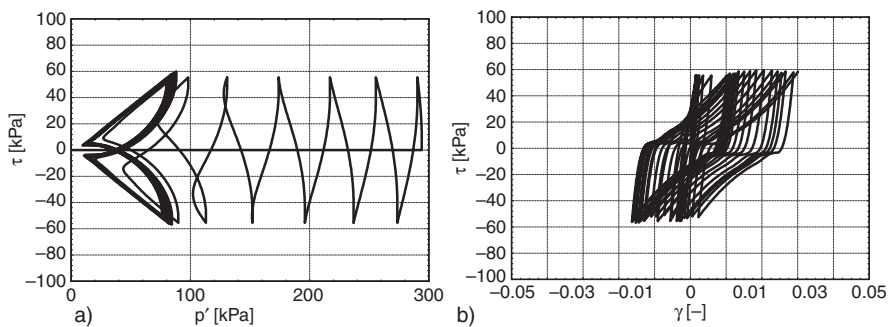


**Fig. 4.4.7.** Simulation of Ishihara and Towhata's (1983) undrained hollow cylinder tests with alternating torque (Fig. 2.10.6) with Sanisand (Niemunis and Prada 2010); (a) skeleton stress path, (b) deviatoric stress-strain curve



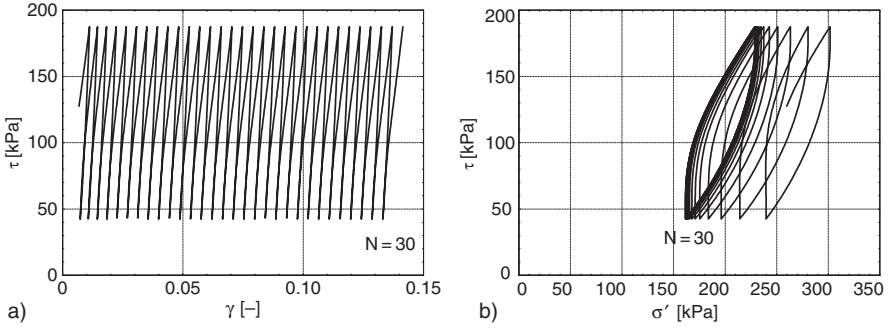


**Fig. 4.4.8.** Simulation of undrained ratcheting in a shearing device (Andersen and Berre 1999, Fig. 2.10.8) with Sanisand (Niemunis and Prada 2010); (a) stress-strain curve, (b) stress path

It appears that only Andersen and Berre (1999) observed *shear ratcheting* (Fig. 2.10.8), though not uniformly with a device as by Fig. 2.10.2a. This is qualitatively reproduced with Sanisand, Fig. 4.4.8. The calculated plot of shear stress vs. shearing (a) and the simulated stress path (b) could be improved by matching parameters, but such a calibration is debatable with the inevitable non-uniformity. As far as a stationary ratcheting is attainable in such tests the model may be considered as validated. The experiment cannot reveal elastic ranges as the device produces a force-roughness which enhances anelastic effects.

To *sum up*, the range of validity of elastoplastic relations with back stress (elp- $\alpha$ ), here represented by a recent version of Sanisand, is rather restricted and could not easily be extended. Drained and undrained triaxial tests with few reversals can be fairly well reproduced, some deviations could be avoided with a better hypoplastic relation. The double flow rule before and after reversals observed by Pradhan et al. (1989) is a part of Sanisand, but there is a strange deviation from these tests which may be attributed to an unintended discontinuity. The simulated approach to butterfly- and lense-like stress cycles by symmetric and asymmetric deviatoric stress cycles, respectively, is apparently realistic, but such observed attractors are distorted by the penetration of grains into the membrane. The intermittent relaxation and densification by isochoric and isobaric deformation cycles, respectively, is not reproduced with elp- $\alpha$ . These attractors could be obtained with limit void ratios as in hyp. The calibration for Sanisand could be improved with attractors. Shear localizations with polarisation (Sect. 8.2) cannot be captured with elp- $\alpha$ .

## 4.5 Hypoplasticity with intergranular strain

Niemunis and Herle (1997) proposed a hypoplastic model with a hidden variable (abbreviated hyp- $\delta$ ) for sand-like soils. This is outlined and discussed here first for cylindrical RSEs. The components  $h_1$  and  $h_2 = h_3$  of the hidden



<http://www.springer.com/978-3-540-36353-8>

Physical Soil Mechanics

Gudehus, G.

2011, XIII, 840 p., Hardcover

ISBN: 978-3-540-36353-8